Gradient-induced vibrations and motion-induced Lenz effects on conductive nonmagnetic orthopedic implants in MRI

Received: 16 April 2024 | Revised: 2 August 2024 | Accepted: 4 August 2024

DOI: 10.1002/mrm.30263

RESEARCH ARTICLE

Magnetic Resonance in Medicine

Gradient-induced vibrations and motion-induced Lenz effects on conductive nonmagnetic orthopedic implants in MRI

Luca Zilberti[1] | **Cristina Curreli**[2] | **Alessandro Arduino**[1] | **Umberto Zanovello**[1] | **Fabio Baruffaldi**[2] | **Oriano Bottauscio**[1]

[1]Istituto Nazionale di Ricerca Metrologica (INRIM), Torino, Italy

[2]Laboratorio di Tecnologia Medica, IRCCS Istituto Ortopedico Rizzoli, Bologna, Italy

Correspondence
Luca Zilberti, Istituto Nazionale di Ricerca Metrologica, Strada delle Cacce 91, I-10135, Torino, Italy.
Email: l.zilberti@inrim.it

Funding information
European Partnership on Metrology, Grant/Award Number: 21NRM05 STASIS

Abstract

Purpose: To quantify the extent of gradient-induced vibrations, and the magnitude of motion-induced displacement forces ("Lenz effect"), in conductive nonmagnetic orthopedic prostheses.

Methods: The investigation is carried out through numerical simulations, for a 3 T scanner. For gradient-induced torques and vibrations, a knee and a shoulder implant are considered, at dB/dt equal to 42 T/s (rms). For motion-induced forces associated with the Lenz effect, a knee and a hip implant are studied, considering a patient who translates on the examination couch, or walks next to it.

Results: Gradient-induced torques may be within the same order of magnitude as the worst case gravitational torque defined in the ASTM standards. However, for all investigated cases, they result to be lower. In vacuum, the extent of the corresponding vibration reduces with frequency. At the lowest investigated frequency (270 Hz), it keeps below 25 μm. For an implant partially embedded in bone, the extent of the vibration increases with frequency. Nevertheless, the displacement is far lower than the worst case observed in vacuum (negligible in contact with the bone; ∼1 μm or less where the implant emerges from the bone). The Lenz effect induced by the motion of the patient through the stationary magnetic field produces forces on the order of a few millinewtons (i.e., at least two orders of magnitude lower than the implant weight).

Conclusion: Comparing the results with mechanical loads caused by ordinary activities of daily living, and with the levels of tolerable micromotions, a good safety margin is confirmed.

KEYWORDS

displacement force, dynamic torques, implants, Lenz effects, Lorentz force, mechanical vibrations

1 | INTRODUCTION

According to ASTM F2503, medical devices that are anticipated to enter the MR environment may be marked as MR Safe, MR Conditional, or MR Unsafe.[1] To identify the proper label, many potential risks have to be investigated. One of them is the possible dislocation of the device, due to mechanical actions exerted by the stationary magnetic field of the MRI scanner. This field can interact with ferromagnetic objects, which are attracted towards the center of the scanner. If the objects are elongated, they also tend to align with the direction of the field.

Another mechanical effect may take place even if the object is nonmagnetic, due to the Lorentz force.[2] The latter originates from the interaction of the stationary magnetic field with an electric current circulating inside the object. In case of passive conductive devices implanted in the patient's body, eddy currents may be the result of electromagnetic induction, which, in MR environments, can be driven by two physical processes. The first is associated with the gradient fields, which, typically, have trapezoidal waveforms. In this case, the eddy currents flow back and forth, following the slope of the gradient field waveform. Thus, the interaction with the stationary magnetic field gives rise to a distribution of Lorentz forces that act back and forth as well, stimulating the vibration of the object.[3,4] This process requires the presence of the gradient field; hence, it can occur inside the scanner, during the application of an MR pulse sequence.

The second process that can trigger electromagnetic induction is the motion of the conductive object through the stationary magnetic field, during patient positioning. In this case, the Lorentz force is generated by the interaction between the stationary magnetic field and the eddy currents induced by the motion through the magnetic field itself. This effect takes place when the patient translates with the examination couch, or walks near the scanner. Unlike gradient-induced eddy currents, motion-induced eddy currents are typically unidirectional, and therefore give rise to push/pull force pulses, instead of vibrations. These pulses tend to counteract electromagnetic induction, according to Lenz law.[5] For this reason, in the literature these mechanical actions are sometimes identified as "Lenz effects" (or "Lenz forces").[6]

The empirical evidence suggests that the risk of injuries associated with gradient-induced vibrations and motion-induced Lenz effects is low. To the authors' knowledge, no accident has ever been ascribed to these mechanical effects. Nevertheless, some attention has been paid to them. A heating sensation was reported by patients wearing cervical fixation devices during MRI. Dedicated investigations put in evidence that the skull pins remained cool but vibrated during the exam. The "drilling" sensation might have been interpreted by the patient as a heating.[7]

Looking at the standards in force, gradient-induced vibrations are discussed in ISO/TS 10974, which provides instructions to evaluate the corresponding harm. However, this standard applies to active implants, and gradient-induced vibrations are considered as a source of malfunction of the device, rather than damage of the surrounding tissues.[8] Despite this, some studies addressing the problem of the potential injury of tissues in the presence of gradient-induced vibrations were carried on. An optical measurement system was developed for the contactless evaluation of gradient-induced vibrations in neuronal implants.[9] This system was used to investigate underdamped behaviors of neural interfaces, putting in evidence the potential risk of amplified vibrations due to on-resonance excitations, which might produce tissue irritation.[10] Gradient-induced vibrations were also investigated for leadless pacemakers, obtaining oscillations that can be considered negligible with respect to those due to the cardiac cycle.[11]

Regarding the forces associated with the Lenz effect, the research focused mainly on the possible braking action undergone by artificial cardiac valves operating in the presence of the stationary magnetic field of MRI scanners.[12–15] In general, these studies agree that, in some cases, the Lenz effect may manifest itself as a resistive pressure comparable to cardiac pressure, which hinders the opening/closing of the valve. The effect is stronger in case of valves with full conducting disks, whose safety in MRI should be carefully evaluated.

Speaking about orthopedic implants, a few references are available. Gradient-induced vibrations and Lenz effects were investigated by Graf et al in 2006.[16] The study focused on torsional moments, using, as a reference threshold, the "worst case gravitational torque" (WCGT) adopted as an acceptance criterion in the ASTM F2213 standard (the standard that covers the measurement of the torque induced by the stationary magnetic field on objects having a non-null magnetic susceptibility).[17] Such a threshold is equal, by definition, to the product of the maximum device dimension and the device weight, and provides a conservative safety limit. Computations applied to simplified geometries (wire frames and plates) predicted dynamic gradient-induced torques that may exceed the WCGT. The presence of such torques was confirmed experimentally on some implants, but only in a qualitative way, without measuring the extent of the vibrations. Gradient-induced torques exceeding the WCGT were also predicted by Nyenhuis, for an acetabular hip shell made of stainless steel.[18]

In the aforementioned paper,[16] Graf et al also evaluated (and observed experimentally) torques associated with the Lenz effect. In general, the intensity of these

torques was low with respect to both the WCGT and the gradient-induced torques, but the authors suggested that the relevance of this phenomenon could increase in the future, depending on the evolution of the MRI technology. Interestingly, the article concentrated on torsional strains, and did not discuss motion-induced displacement forces. The latter, according to some authors, might be perceived and reported by the patient, creating the wrong concern that the implant has ferromagnetic parts (possibly leading to the cancelation of the exam).[6,19] Regarding this, standard ASTM F2052 (the standard that covers the measurement of the displacement force induced by the stationary magnetic field on objects having a non-null magnetic susceptibility)[20] recommends using the weight of the object as a conservative reference to evaluate the risk. By analogy, the same criterion might be used to assess the risk related to the forces due to the Lenz effect in conductive nonmagnetic implants.

In this paper, we use numerical simulations to deepen the investigation of both gradient-induced torques and Lenz effects on bulky orthopedic implants, with a twofold objective. For gradient-induced torques, the aim is to estimate the extent of the vibrations produced on the implants. For the Lenz effect, the aim is to quantify the net force exerted on the implants and compare it with the stress that occurs in daily life. In both cases, the attention is entirely concentrated on the Lorentz force driven by the eddy currents. Possible mechanical effects due to a non-null magnetic susceptibility of the materials are therefore disregarded.

Our findings confirm the common belief about the absence of significant risks for the tissues surrounding the implants. Nevertheless, we believe that a rigorous quantification is beneficial. On the one hand, because it allows identifying the width of the current safety margin, in view of future developments of the MRI technology. On the other hand, because of its pedagogical value.

2 | METHODS

2.1 | Analytical solution for gradient-induced vibrations

The investigation of gradient-induced vibrations was conducted preliminarily through the following analytical solution, useful to put in evidence the effect of some parameters.

Let us consider a conductive, nonmagnetic, homogeneous sphere, with radius R, sketched in Figure 1. The sphere has magnetic permeability μ_0, electrical conductivity σ and mass density δ. The sphere is subjected to a homogeneous, time-harmonic, magnetic induction $\boldsymbol{B}_G$

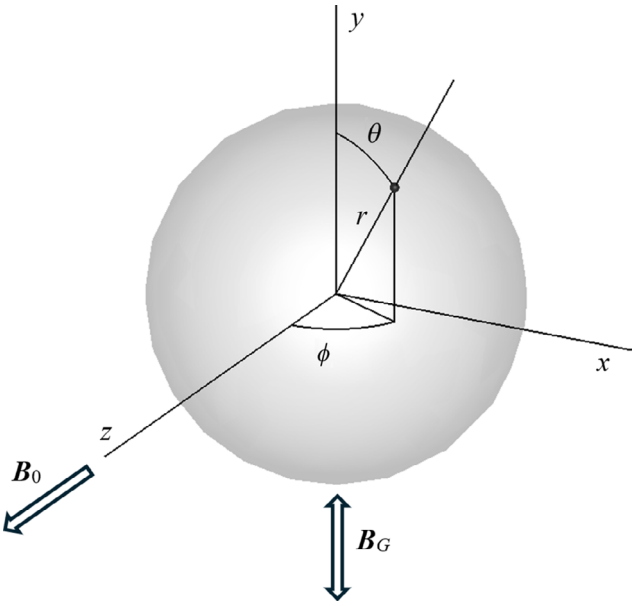

FIGURE 1 Geometry adopted in the analytical description of gradient-induced vibrations in a homogeneous sphere. The time-harmonic magnetic induction $\boldsymbol{B}_G$ (used to represent the gradient field) oscillates along the y axis, whereas the stationary magnetic induction $\boldsymbol{B}_0$ is directed along the z axis. Colatitude and longitude are indicated by θ and ϕ, respectively.

(intended to represent the gradient field), directed along the y direction, oscillating at frequency f. The analytical description of the current density $\boldsymbol{J}$ induced in the sphere, written in complex notation, is known.[21] When R is small with respect to the penetration depth of the field in the material (a condition that occurs for sufficiently low values of the product σf),[22] the "skin effect" may be neglected and the current density can be safely approximated as

$$\boldsymbol{J} = \pi\sigma f B_G r \sin\theta \, \mathbf{u}_\phi, \tag{1}$$

where r is the distance of the considered point from the sphere center, θ is the colatitude (measured from the y axis), and ϕ is the longitude (measured in the zx plane, from the z axis). Symbol $\mathbf{u}$ indicates a basis unit vector. The current density in Eq. (1) has azimuthal direction (i.e., it circulates around the y axis). For reasonable frequency values (up to about 10 kHz), the penetration depth in the alloys commonly used to manufacture orthopedic implants is on the order of some centimeters.[21] This corroborates the validity of the approximation adopted in Eq. (1).

Let us now assume that the sphere is also immersed in a homogeneous stationary magnetic induction $\boldsymbol{B}_0$, directed along the z direction (i.e., perpendicular to $\boldsymbol{B}_G$). The volume density of the Lorentz force is

$$\boldsymbol{F}_v = \boldsymbol{J} \times \boldsymbol{B}_0 = -\pi\sigma f B_G B_0 r \sin\theta \quad \cos\phi \mathbf{u}_y. \tag{2}$$

Due to symmetry, the volume integral of $\boldsymbol{F}_v$ is null. Thus, there is no net force acting on the sphere. However, the sphere is subjected to a torque density equal to

$$\boldsymbol{T}_v = \boldsymbol{r} \times \boldsymbol{F}_v = \pi \sigma f B_G B_0 r^2 (\sin\theta)^2 \cos\phi \left[\cos\phi \mathbf{u}_x - \sin\phi \mathbf{u}_z\right]. \tag{3}$$

Integrated over the spherical volume, this torque density gives the total torque acting on the sphere, evaluated with respect to its center:

$$\boldsymbol{T} = \int_0^{2\pi}\int_0^{\pi}\int_0^{R} \boldsymbol{T}_v \left(r^2 \sin\theta\right) dr d\theta d\phi = \frac{4}{15} R^5 \pi^2 \sigma f B_G B_0 \mathbf{u}_x. \tag{4}$$

Complex notation implies that all quantities calculated in Eqs. (1)–(4) oscillate at frequency f. Hence, the sphere is forced to oscillate back and forth around the x axis. For the sphere, the moment of inertia (i.e., the ratio between the instantaneous value of the torque and the instantaneous value of the angular acceleration) is

$$I = \frac{8}{15}\pi \delta R^5. \tag{5}$$

If the sphere is free to move without constraints (i.e., it is subjected to its inertia only), in the harmonic regime we have

$$T = I(2\pi f)^2 \Omega, \tag{6}$$

where Ω is the amplitude of the oscillation angle. Thus, the latter results to be

$$\Omega = \frac{\sigma B_G B_0}{8\pi f \delta}. \tag{7}$$

This angle increases with the amplitude of both applied fields, and decreases with density. Under the adopted approximation, it decreases linearly with frequency and does not depend on the sphere size. In Eqs. (4) and (7), f and B_G are considered as independent parameters. Their product is proportional to the maximum (or the rms) value of dB/dt of the gradient field. Hence, the torque in Eq. (4) is proportional to such a quantity as well. Based on Eq. (7), if one expresses B_G in terms of the rms value of dB/dt, the amplitude of the oscillation angle results to be proportional to the inverse of the square of the frequency:

$$\Omega = \frac{\sigma B_0}{8\pi\delta} \frac{\sqrt{2}}{2\pi} \left(\frac{dB}{dt}\right)_{\text{rms}} \frac{1}{f^2}. \tag{8}$$

The formula in Eq. (1) is valid for a sphere that does not move. Whenever a gradient-induced vibration takes place, it necessarily implies the onset of a Lenz effect, which produces additional electromagnetic induction and influences the motion itself. According to Lenz law, this additional effect always acts as a viscous drag, reducing the amplitude of the oscillation angle Ω. Hence, conservative results are obtained if it is neglected. As shown below (see the Results section), the amplitude of the oscillation angle calculated through Eq. (7) is small for realistic values of the parameters. Additional analytical and numerical calculations, not reported for brevity, shows that the braking torque acting on the sphere due to the additional Lenz effect amounts to about 1 % of the gradient-induced torque. Hence, the additional Lenz effect may be seen as a "higher order" correction, which does not modify the results significantly.

2.2 | Numerical simulations of gradient-induced vibrations

Electromagnetic simulations were performed, under time-harmonic conditions, using the magnetoquasistatic frequency domain solver of the CST software.[23] Two metallic, nonmagnetic, orthopedic implants were considered: a right shoulder prosthesis designed for hemiarthroplasty and a left knee implant suitable for total arthroplasty, including femoral and tibial components.[24] For simplicity, the prostheses were assumed to be entirely composed of Ti6Al4V alloy ($\sigma = 0.58$ MS/m, $\delta = 4420$ kg/m^3). Their features are collected in Table 1.

For the sake of generality, and considering that the size of the implants is relatively small, the field produced by the gradient coils was simulated as a uniform field. This avoids binding the results to a specific coil design. To get results of practical interest, the implants were oriented in space to simulate the orientation they would have in case of a patient placed supine inside a tubular scanner. The time-harmonic field was applied either along the x (lateral), y (vertical), or z (longitudinal) direction, thus considering the possible action of the concomitant components. Following ISO/TS 10974,[8] the rms value of dB/dt was set to 42 T/s. We notice that, based on a survey involving commercial scanners, this should be the highest value that can take place in the volume accessible to the patient (in positions $|x| \sim 23$ cm, $|z| \sim 30$ cm, which are likely outside the FOV, but relevant for safety, anyway), achieved when running TrueFISP or echo-planar sequences.[8] The amplitude B_G was set, conservatively, to 35 mT. This resulted in a frequency of 270 Hz.

The simulations provided the distribution of the current density induced in the metallic objects. The volume density of Lorentz force was obtained as the vector product of the current density and a uniform, z-directed, stationary magnetic induction equal to 3 T (this is a reasonable assumption, considering that the adopted 42 T/s value can take place in points where $\boldsymbol{B}_0$ is almost perfectly

homogeneous and longitudinal). The spatial distribution of the force density was used as an input for the mechanical simulation, performed, in harmonic regime, using the software Ansys Mechanical.[25] Finite Element models of the implants were developed, applying a tetrahedral mesh. The Ti6Al4V alloy was modeled as an elastic isotropic material, with Young modulus and Poisson ratio of 110 GPa and 0.32, respectively. To keep the problem simple, the mechanical response of the implants was first evaluated in a vacuum, where the extent of the vibration is limited by the periodic change in the sign of the applied torque. To extend the analysis, the simulation of the shoulder implant exposed to an x-directed $\boldsymbol{B}_G$ field was repeated at 500 Hz and 1750 Hz, keeping dB/dt rms equal to 42 T/s (i.e., setting B_G equal to 18.9 mT and 5.40 mT, respectively). To get a rough quantification of the damping effect due to the tissues, these simulations were further repeated, embedding the stem of the shoulder implant within a cylinder with average mechanical properties of cortical bone (Young modulus: 16.7 GPa; Posson ratio: 0.3).[26] The interface between the implant and the bone was simulated as a bonded contact, which prevented any creep at the bone-implant interface. No tissue was placed around the implant head.

2.3 | Numerical simulations for motion-induced Lenz effect

Motion-induced Lenz effects were simulated using a homemade code, validated and described in a previous paper,[27] implemented to investigate motion-induced electric fields in a body moving through the fringe field of MRI scanners.[28] The same knee implant considered for gradient-induced vibrations was simulated. In addition, a left hip implant composed of stem and acetabular cup,[24] both made of Ti6Al4V, was simulated (see Table 1). In order to move these implants along realistic trajectories, they were placed in the left leg of the Glenn body model,[29] following a "virtual surgery" procedure.[24]

The human model with prostheses was moved through the stationary magnetic field generated by a realistic model of a 3 T actively shielded magnet. The latter is composed of 13 circular coils, symmetric with respect to the central xy plane, with the longitudinal axis located 1 m above the floor. Two motion trajectories, indicated with A and B, were simulated. Trajectory A implied the translation of the body placed supine on the examination couch. At the starting position, the head of the body was placed just outside the scanner entrance. Then, a longitudinal 2.3 m translation was performed, at a quite high speed of 0.3 m/s, inside the scanner. At the final position, the knee prosthesis reached the center of the scanner. Trajectory B was conceived to simulate the motion of a patient who walks towards the scanner bore, with the leg carrying the prostheses moving next to the examination couch. A 1.5 m longitudinal translation was performed, at the speed of 1 m/s, keeping the vertical axis of the body at $x = -0.55$ m. At the final position, the face of the human model was close to the frontal surface of the scanner. Figure 2 sketches the position of the two implants with respect to the scanner, for both trajectories. Figure 3 shows the Cartesian components of $\boldsymbol{B}_0$ for the simulated scanner, on two planes that span the range of motion of the two trajectories.

The computational code provided the distribution of the current density induced in the metallic implants. At each instant, this current density was used, together with the local value of $\boldsymbol{B}_0$, to obtain the volume density of the Lorentz force. The latter, integrated on the volume of the implants, provided the time-behavior of the net force due to the Lenz effect.

3 | RESULTS

3.1 | Extent of gradient-induced vibrations

Eq. (7) has been used to calculate the oscillation angle of a sphere made of Ti6Al4V, immersed in a stationary magnetic field ($B_0 = 3$ T) and exposed to a time-harmonic magnetic field perpendicular to it ($B_G = 35$ mT, $f = 270$ Hz). Angle Ω results to be about 2 mrad (i.e., 0.116°). For a sphere with a radius of 2 cm (similar to the femoral head

TABLE 1 Physical features of the considered orthopedic implants made of Ti6Al4V alloy.

Implant	Component	Volume (cm^3)	Maximum linear dimension (cm)	Weight (mass)
Shoulder	-	21.7	11.7	941 mN (95.9 g)
Knee	Femoral	36.8	7.5	1600 mN (163 g)
	Tibial	11.8	6.8	513 mN (52.3 g)
Hip	Acetabular cup	14.9	5.2	645 mN (65.8 g)
	Stem and ball	55.2	17.0	2390 mN (244 g)

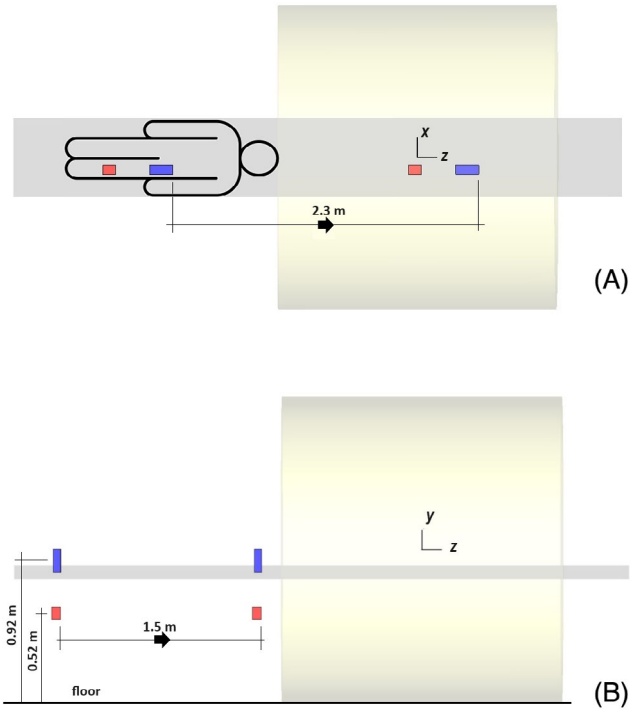

FIGURE 2 Scheme of the two trajectories simulated to study the Lenz effect, including the initial and final positions of the bounding boxes of the hip implant (blue rectangle) and knee implant (red rectangle). Upper plot: Trajectory A (translation of the body placed supine on the examination couch; top view); speed: 0.3 m/s; total displacement: 2.3 m. Lower plot: Trajectory B (patient who walks towards the scanner bore; lateral view); speed: 1 m/s; total displacement: 1.5 m. In both images, the position of the isocenter and the direction of the Cartesian reference frame are indicated. The direction of the motion is indicated by the black arrow. The position of the prostheses within the body is sketched in the upper plot. The height of the prostheses with respect to ground is indicated, for the standing patient, in the lower plot.

of a hip implant), such a vibration corresponds to a maximum linear displacement of 40 μm (i.e., 80 μm for the entire span of the oscillation). This analytical solution has been used to validate the numerical model used to investigate the behavior of more realistic objects, obtaining an excellent agreement (discrepancy lower than 1 %).

Table 2 shows the magnitude of the Cartesian components (T_x, T_y, T_z) of the torque acting on the shoulder and knee implants (using the center of mass as a reference point). Values are given for the three directions of the applied time-harmonic magnetic field. In each case, the rms value of dB/dt is equal to 42 T/s. The value of the WCGT is also reported, for comparison. In all cases, the gradient-induced torque is weaker than the WCGT. The maximum displacement caused by the vibration at 270 Hz, when the implants are placed in vacuum, is reported in Table 3. The table also indicates the part of the implants where it takes place. Since an almost perfectly rigid rotation around the center of mass occurs, the maximum displacement occurs at the point that is farthest from the axis of rotation. Maximum torques and displacements are similar for the two implants. The highest values are found for the femoral part of the knee prosthesis, when $\boldsymbol{B}_G$ is directed along the y direction. In this case, the strongest torque component is T_x.

Figure 4 shows the behavior of the shoulder implant, in terms of maximum displacement, for three frequencies of the driving term (270 Hz, 500 Hz and 1750 Hz), keeping the same rms value of dB/dt (42 T/s) and applying $\boldsymbol{B}_G$ along the x direction. The results are reported for the case of the implant placed in vacuum (blue circles) or with the stem embedded in a cylinder of bone (orange diamonds). In vacuum, the maximum displacement occurs at the tip of the stem. It amounts to 19.1 μm, 5.81 μm and 1.04 μm for the three frequencies, respectively. This trend is decreasing. However, it does not strictly follow the f^{-2} scaling rule described by Eq. (8), indicating that, as f increases, the motion is no longer perfectly rigid (i.e., some deformation occurs). When the prosthesis is partially embedded in bone, the displacement of the tip of the stem is almost nullified. By virtue of the material elasticity, the implant head, which is not embedded in bone, undergoes the largest displacement. The latter amounts to 0.234 μm at 270 Hz, and then increases to 0.245 μm at 500 Hz and 1.06 μm at 1750 Hz.

3.2 | Amplitude of motion-induced forces due to the Lenz effect

Figures 5 and 6 show the net forces acting on the hip and knee implants, composed of Ti6Al4V alloy, along trajectories A and B, respectively. The Cartesian components of the force (expressed in the reference frame of the scanner) and its norm are displayed. In all cases, the z-component is prevailing, but x- and y-components can be also observed. For trajectory A, the peak of the force occurs when the implants enter the bore and pass through the first coils embedded in the scanner. This roughly occurs at 1 m from the initial position for the hip implant, and at 1.45 m for the knee implant. For the patient on the examination couch, the strongest force acts on the femoral part of the knee implant. For trajectory B, the force is monotonic and reaches the maximum value at the end of the motion, when the patient faces the frontal wall of the scanner. For the patient walking towards the bore, the strongest force acts on the stem and ball of the hip implant. Comparing the results of trajectories A and B, the peak of the forces are higher for the former.

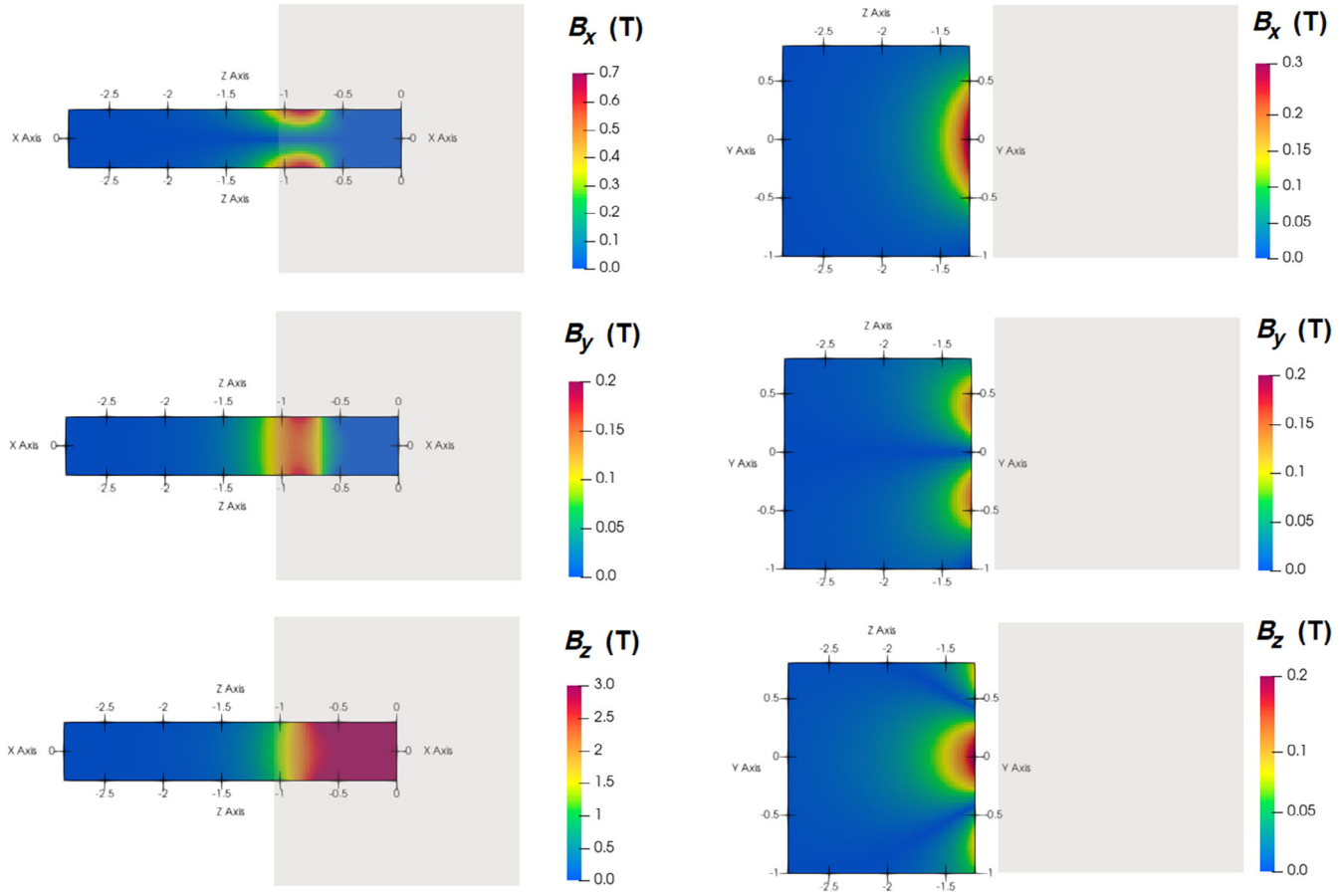

FIGURE 3 Magnitude of the Cartesian components of the stationary magnetic induction produced by the scanner simulated to study the Lenz effect (x-, y- and z-component, from top to bottom). Left side: 2D maps (top view) on a plane at $y = -0.05$ m, covering trajectory A. Right side: 2D maps (lateral view) on a plane at $x = -0.45$ m, covering trajectory B. Each map has its own color scale. The volume taken up by the scanner is indicated by the gray rectangle. The origin of the reference frame is at the center of the scanner.

TABLE 2 Gradient-induced torque for the shoulder and knee implants made of Ti6Al4V alloy, evaluated with respect to the center of mass.

Implant	Worst case gravitational torque (N m)	Direction of the applied magnetic field	T_x (N m)	T_y (N m)	T_z (N m)
Shoulder	0.110	x	6.52×10^{-3}	4.07×10^{-2}	7.43×10^{-6}
		y	2.49×10^{-2}	6.52×10^{-3}	1.45×10^{-5}
		z	6.97×10^{-3}	1.69×10^{-2}	2.40×10^{-5}
Knee kemoral	0.120	x	1.59×10^{-3}	7.65×10^{-3}	1.47×10^{-5}
		y	6.63×10^{-2}	1.59×10^{-3}	1.32×10^{-5}
		z	1.59×10^{-2}	6.24×10^{-4}	1.63×10^{-4}
Knee tibial	0.0349	x	3.94×10^{-7}	5.36×10^{-3}	1.53×10^{-5}
		y	1.13×10^{-2}	3.46×10^{-6}	8.85×10^{-6}
		z	6.18×10^{-3}	3.74×10^{-6}	2.23×10^{-5}

Note: The maximum gravitational torque is, by definition, the product of the weight and the maximum linear dimension of the object, as for Standard ASTM F2213-17. In all cases, the applied harmonic magnetic field (dB/dt rms: 42 T/s) is superposed to a uniform z-directed stationary magnetic field of 3 T.

TABLE 3 Maximum amplitude of vibration for the shoulder and knee implants made of Ti6Al4V alloy, placed in vacuum, at 270 Hz.

Implant	Direction of the applied magnetic field	Maximum displacement (μm)	Position of maximum displacement
Shoulder	x	19.1	Tip of the stem
	y	13.4	Tip of the stem
	z	8.50	Tip of the stem
Knee femoral	x	2.22	Top surface of the medial posterior flange
	y	21.6	Top surface of the anterior flange
	z	4.34	Top surface of the anterior flange
Knee tibial	x	3.99	Lateral edge of the tibial plate
	y	14.2	Tip of the tibial stem
	z	7.82	Tip of the tibial stem

Note: In all cases, the applied harmonic magnetic field (dB/dt rms: 42 T/s) is superposed to a uniform z-directed stationary magnetic field of 3 T. The maximum displacement is evaluated for the combined action of the Cartesian components of the torque, with respect to the original position of the implant. In the whole period of vibration, the entire range of motion is double.

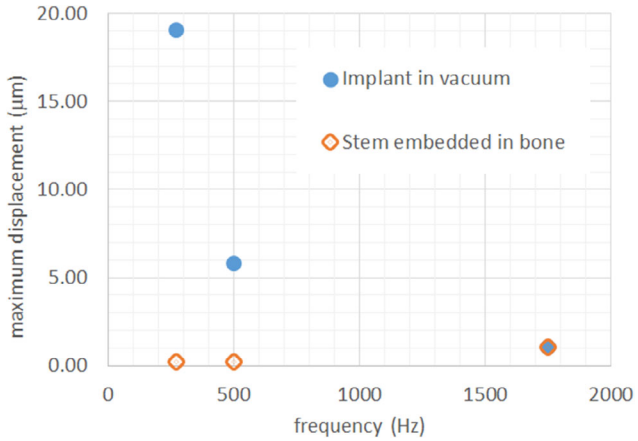

FIGURE 4 Maximum displacement that occurs during the vibration of the shoulder implant when it is exposed to a z-directed stationary magnetic induction of 3 T and an x-directed time-harmonic field (rms value of dB/dt: 42 T/s), at three different frequencies (270 Hz, 500 Hz and 1750 Hz). The cases of the implant placed in vacuum (blue circles) and with the stem embedded in a cylinder of bone (orange diamonds) are compared. In the first case, the maximum displacement occurs at the tip of the stem. In the other case, it takes place on the spherical surface of the implant head, which is not embedded in the bone. The maximum displacement is evaluated with respect to the original position of the implant. The entire span of the oscillation is double.

In all cases, the peak of the force is at least two orders of magnitude lower than the weight of the corresponding implant component, reported in Table 1.

The torques acting on the implants, not reported for brevity, are also far lower than the WCGT (the highest torque has been obtained on the acetabular cup along trajectory A; its peak amounts to about 2 % of the corresponding WCGT).

4 | DISCUSSION AND CONCLUSIONS

4.1 | Extent of gradient-induced vibrations

Under the domain of validity of the adopted approximations (reasonable for the present investigation, as discussed previously) the analytical solution clarifies the role played by the different parameters. Specifically, the extent of the vibration is:

- proportional to σ, B_G and B_0;
- inversely proportional to δ and, under the assumption of a rigid motion that takes place without mechanical constraints, to f.

Notably, working in terms of dB/dt rms (which links B_G and f) the extent of the vibration becomes proportional to f^{-2} for a rigid motion.

For the Ti6Al4V implants, some of the calculated torques have the same order of magnitude of the WCGT, but they are always lower (in the worst case reported in Table 2, the magnitude of the gradient-induced torque is about one half of the WCGT). This result has been obtained for a high dB/dt rms value (42 T/s). Stronger torques, potentially exceeding the WCGT, would take place in stronger B_0 fields (e.g., at 7 T). However, torques higher than the WCGT do not necessarily represent a danger. Indeed, although torque is a practical metric, the real mechanical effect is the displacement undergone by the implants. Moreover, it must be remarked that the WCGT defined in ASTM F2213-17 is a static torque, whereas gradient-induced torques are dynamic

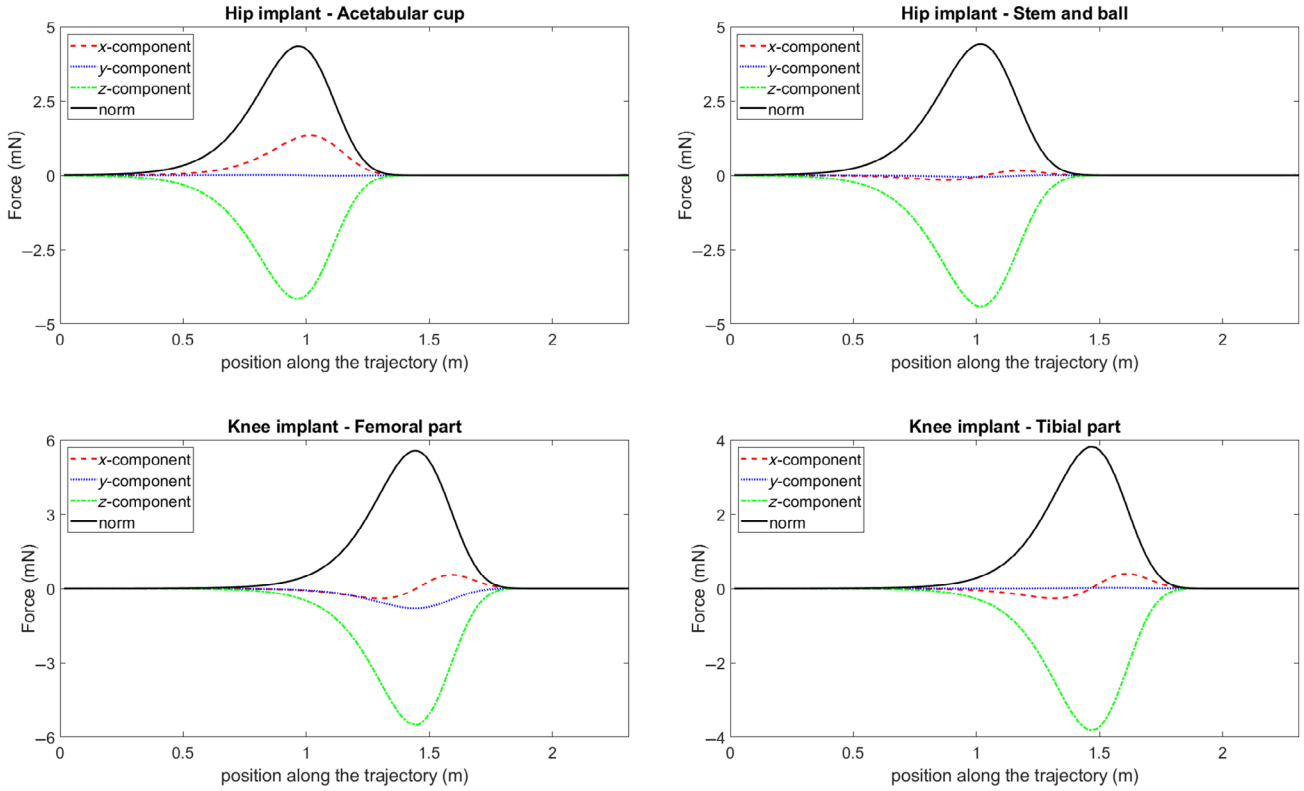

FIGURE 5 Net force acting on the Ti6Al4V implants, due to the Lenz effect, as a function of the position along trajectory A (translation of the body placed supine on the examination couch). Upper left: Acetabular cup of the hip implant; upper right: Stem and ball of the hip implant; lower left: Femoral part of the knee implant; lower right: Tibial part of the knee implant. Each graph reports the Cartesian components of the force and the norm.

and their effect changes with frequency. Potentially, micromotions at the implant-bone interface represent a danger for the tissues (e.g., due to inflammatory reactions) and for implant stability.[30] At early post-operative stages, excessive micromotions may create conditions for implant failure.[30–34] Because of its dependence on many factors, no general consensus exists about the lower threshold for critical micromotion.[30,34] In some cases, implant loosening was ascribed to micromotions as low as 30 μm.[30,34] In general, micromotions in excess of 150 μm are accepted to inhibit osseointegration, facilitating the development of fibrous tissue rather than bony ingrowth.[30,32,33]

For the shoulder implant with the stem embedded in bone, the maximum gradient-induced displacement increases with frequency, indicating that bone becomes less effective in limiting the extent of the vibration (and suggesting the possibility that a mechanical resonance exists). Despite this, the displacement is always small (1 μm or less for the implant head; far less for the stem). Even if this result is probably affected by some underestimations (because of the use of a bonded contact at the implant-bone interface, and the adoption of a homogenous stiffness in the bone),[30,35] it suggests that gradient-induced vibrations produce negligible micromotions in case of good levels of osseointegration.

In vacuum, at constant dB/dt rms, the displacement is maximized at the lowest frequency (270 Hz). This configuration, in which no constraint is applied, gives an upper limit, which should cover conservatively the cases of failed osseointegration (where the implant is surrounded by a periprosthetic layer, much less rigid than mineralized bone). In the worst case (femoral part of knee implant, with $\boldsymbol{B}_G$ along y) the maximum displacement amounts to 21.6 μm, corresponding to a full range of motion of 43.2 μm. Similar values, which can take place during the healing phase if ordinary loads are applied,[36] are still considered to be in the safe range by many studies.[31–33] Taking into account the wide level of overestimation of the adopted model, these results lead to the conclusion that an impairment of the osseointegration due to gradient-induced vibrations is unlikely at 3 T.

Before concluding, it is interesting to discuss what would occur for CoCrMo, which is another alloy commonly adopted for orthopedic prostheses. The conductivity of CoCrMo ($\sigma = 1.16$ MS/m) is almost double with respect to the conductivity of Ti6Al4V. Hence, for the same applied fields and implant geometry, the value of the

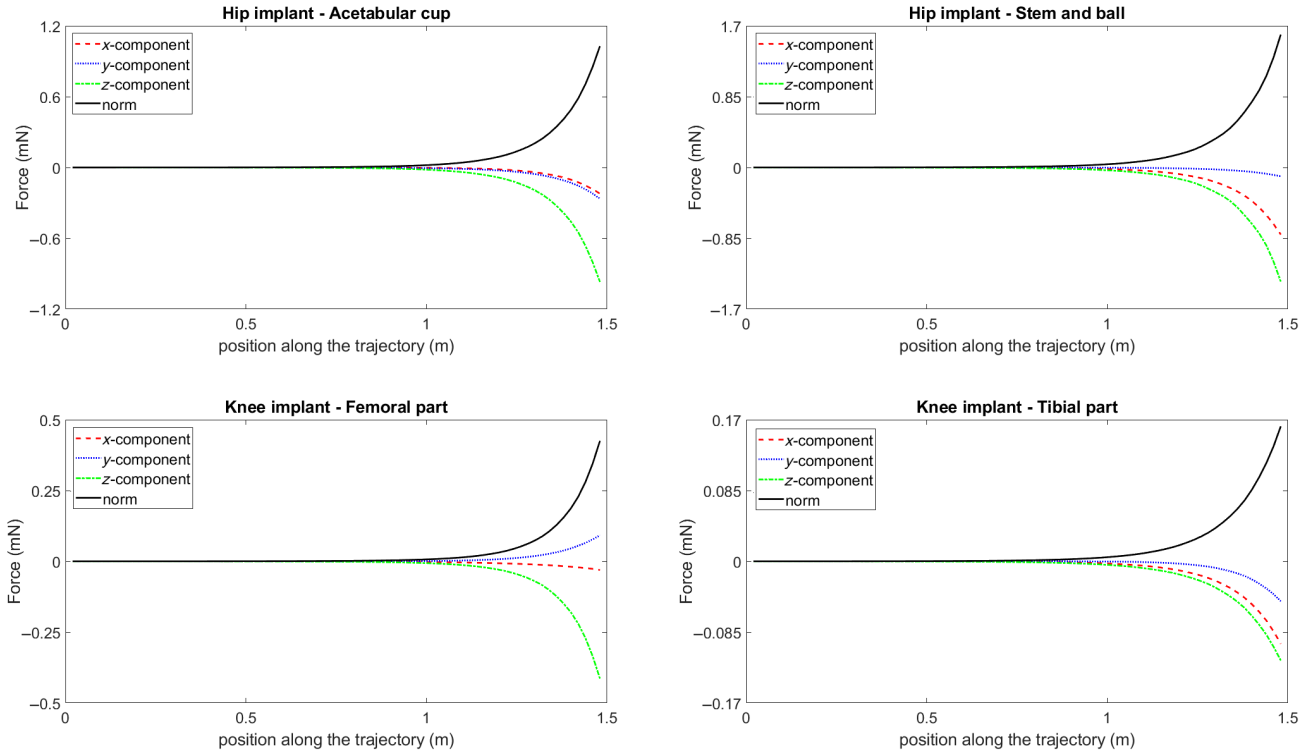

FIGURE 6 Net force acting on the Ti6Al4V implants, due to the Lenz effect, as a function of the position along trajectory B (patient who walks towards the scanner bore). Upper left: Acetabular cup of the hip implant; upper right: Stem and ball of the hip implant; lower left: Femoral part of the knee implant; lower right: Tibial part of the knee implant. Each graph reports the Cartesian components of the force and the norm.

gradient-induced torque would be double for this material. Incidentally, also the density of CoCrMo is about double ($\delta = 8445\,\mathrm{kg/m^3}$), meaning that the WCGT used as a term of comparison doubles as well. Moreover, also the moment of inertia doubles. Thus, the amplitude of the oscillation in vacuum, according to Eqs. (6), (7), would keep almost the same as that reported for Ti6Al4V.

Some simplifications adopted in this study are worth remarking. First, the role played by the parameters in the electromagnetic problem has been discussed, for the sake of simplicity, neglecting the skin effect. This produces conservative torque values. The direction of $\boldsymbol{B}_0$ has been chosen to represent only the most common situation, in which it is directed along z. For the uniform time-harmonic field intended to represent the gradient field, the direction has been set along x, y, or z. This should have produced a quite general overview of the problem, but it does not provide, strictly speaking, a maximization of the mechanical effect. Finally, the simulation of the shoulder implant partially embedded in bone does not provide a detailed mechanical model of the real anatomy (particularly, in the post-operative healing phase). To get more accurate quantifications, advanced models are therefore required, especially to investigate possible resonant behaviors and imperfect osseointegration situations.

4.2 | Amplitude of motion-induced forces due to the Lenz effect

The forces that act during the translation of the patient on the examination couch have a prevailing z-component, with negative sign. Such a component acts to oppose the motion (which occurs parallel to the positive z-axis). Specifically, the mechanical action tries to oppose the increase of the field experienced by the prostheses, which becomes stronger as the implants approach the bore. Once the implants are at the center of the scanner, further motion does not correspond to any field variation and the braking effect ceases. Similarly, a viscous drag directed along the negative z-axis acts also during the motion of the patient who walks towards the scanner (which is again parallel to the z-axis). In this case, the force is monotonic and goes on increasing until the motion stops. For both trajectories, minor force components, acting along the x and y directions, are also present. In some cases (e.g., the acetabular cup, along trajectory A) such forces "pull" the object towards the axis of the scanner. We notice that, if these forces succeeded, they would deviate the trajectory of the implants towards regions where the field is more homogeneous. As a result, the variation of the linkage magnetic flux would be mitigated, consistently with Lenz

law. Concerning this, we remind that the value of the linkage flux depends on the local direction of the magnetic field and on the geometry of the object. Due to the relatively complicated shape of the implants, it may not be straightforward to predict the sign of the forces that act transversally with respect to the direction of the motion.

The Lenz effect depends on the spatial gradient of $\boldsymbol{B}_0$. The latter is determined by the design of the main magnet (including passive or active shielding). In general, each magnet model has its own field pattern, which requires a dedicated simulation to produce specific results. With respect to the conductivity of the implants, the problem is linear. If the investigated implants were composed of the CoCrMo alloy, which has a conductivity double than Ti6Al4V, the forces would double as well. Finally, the magnitude of the motion-induced eddy currents is proportional to the speed of motion and this proportionality reflects on the Lorentz force. In Figures 5 and 6 the forces are displayed as a function of the position. If, for the same trajectory, the speed doubles, the values of the forces in the graphs double, whereas the values in the abscissa keep the same. However, the duration of the motion would halve (i.e., the force pulses would be stronger and shorter). Whereas the speed in trajectory B could be increased (e.g., to simulate a person who walks faster, or runs), the speed of the MRI bed adopted in trajectory A is already quite conservative (even if feasible, in many scanners).

For all investigated cases, the forces result to be far lower than the weight of the implants. Specifically, the highest force is about 6 mN (corresponding to less than 1 g, in terms of equivalent gravitational mass). As discussed, the possibility to perceive the Lenz effect enhances at the increase of conductivity, of the speed of motion, and of the gradient of the fringe field. Thus, this study cannot claim to provide a fully exhaustive assessment. Nevertheless, for patients moving in the field of a 3 T tubular scanner, the observed safety margin seems to be large enough to exclude any damage to tissues. Indeed, the latter should be perfectly able to retain the implant in the proper position considering that, during activities of daily living, forces on knee and hip joints commonly exceed the body weight.[30,37,38]

In a safety perspective, the reduction of the speed of motion is a practical and effective way to minimize the Lenz effect (and possible annoying sensations), anyway.

ACKNOWLEDGMENTS

The results presented here have been developed in the framework of the 21NRM05 STASIS Project. The Project has received funding from the European Partnership on Metrology, co-financed from the European Union's Horizon Europe Research and Innovation Programme and by the Participating States. The authors acknowledge the support of Zurich MedTech in the development of the human model with implants. CAD models of hip and knee implants were kindly provided by the manufacturer of prosthetic devices Adler Ortho® SpA, Italy (www.adlerortho.com). Open access publishing facilitated by Istituto Nazionale di Ricerca Metrologica, as part of the Wiley - CRUI-CARE agreement.

DATA AVAILABILITY STATEMENT

The data sets of results will be made publicly available on Zenodo (10.5281/zenodo.12569940).

ORCID

Luca Zilberti https://orcid.org/0000-0002-2382-4710
Alessandro Arduino https://orcid.org/0000-0002-4829-5130
Umberto Zanovello https://orcid.org/0000-0001-6415-9967
Oriano Bottauscio https://orcid.org/0000-0002-5437-4396

REFERENCES

1. ASTM International. *ASTM F2503-23 Standard Practice for Marking Medical Devices and Other Items for Safety in the Magnetic Resonance Environment*. ASTM; 2023.
2. Fagan AJ, Bitz AK, Björkman-Burtscher IM, et al. 7T MR safety. *J Magn Reson Imaging*. 2021;53:333-346.
3. Delfino JG, Woods TO. New developments in standards for MRI safety testing of medical devices. *Curr Radiol Rep*. 2016;4:28.
4. Panych LP, Madore B. The physics of MRI safety. *J Magn Reson Imaging*. 2018;47:28-43.
5. International Electrotechnical Commission (IEC). *IEC 60601–2-33 Medical Electrical Equipment – Part 2–33: Particular Requirements for the Basic Safety and Essential Performance of Magnetic Resonance Equipment for Medical Diagnosis, Edition 4.0*. IEC; 2022.
6. ACR Committee on MR Safety. *ACR Manual on MR Safety, Version 1.0*. American College of Radiology; 2020.
7. Hartwell RC, Shellock FG. MRI of cervical fixation devices: sensation of heating caused by vibration of metallic components. *J Magn Reson Imaging*. 1997;7:771-772.
8. International Organization for Standardization (ISO). *ISO/TS 10974 Assessment of the Safety of Magnetic Resonance Imaging for Patients with an Active Implantable Medical Device*. 2nd ed. ISO; 2018.
9. Fuhrer E, Jouda M, Gruschke OG, Korvink JG. Optical gauge head to evaluate gradient field induced vibrations of conductive structures during MRI. *In 2017 International Conference on Electromagnetics in Advanced Applications (ICEAA)*, Verona, Italy. IEEE; 2016. doi:10.1109/ICEAA.2017.8065581
10. Fuhrer E, Jouda M, Klein CO, Wilhelm M, Korvink JG. Gradient-induced mechanical vibration of neural interfaces during MRI. *IEEE Trans Biomed Eng*. 2020;67:915-923.
11. Childers M, Sethna D, Sison S. MRI gradient induced vibration of leadless pacemakers. *In 2023 ISMRM & ISMRT Annual Meeting & Exhibition*, Toronto, Canada. International Society for Magnetic Resonance in Medicine; 2023 Abstract 2875.

12. Condon B, Hadley DM. Potential MR Hazard to patients with metallic heart valves: the Lenz effect. *J Magn Reson Imaging*. 2000;12:171-176.
13. Robertson NM, Diaz-Gomez M, Condon B. Estimation of torque on mechanical heart valves due to magnetic resonance imaging including an estimation of the significance of the Lenz effect using a computational model. *Phys Med Biol*. 2000;45:3793-3807.
14. Golestanirad L, Dlala E, Wright G, Mosig JR, Graham SJ. Comprehensive analysis of Lenz effect on the artificial heart valves during magnetic resonance imaging. *Prog Electromagn Res*. 2012;128:1-17.
15. Edwards MB, Mclean J, Solomonidis S, Condon B, Gourlay T. In vitro assessment of the Lenz effect on heart valve prostheses at 1.5 T. *J Magn Reson Imaging*. 2015;41:74-82.
16. Graf H, Lauer UA, Schick F. Eddy-current induction in extended metallic parts As a source of considerable torsional moment. *J Magn Reson Imaging*. 2006;23:585-590.
17. ASTM International. *ASTM F2213-17 Standard Test Method for Measurement of Magnetically Induced Displacement Force on Medical Devices in the Magnetic Resonance Environment*. ASTM; 2017.
18. Nyenhuis JA. Heating and torque of passive metallic implants by gradient dBdt and static field B0 in MRI. Proceedings of the 2020 ISMRM & SMRT Virtual Conference & Exhibition. *International Society for Magnetic Resonance in Medicine*; 2020:4212.
19. Shellock FG, Rosen MS, Webb A, et al. Managing patients with unlabeled passive implants on MR systems operating below 1.5 T. *J Magn Reson Imaging*. 2023;59:1514-1522. doi:10.1002/jmri.29002
20. ASTM International. *ASTM F2052-21 Standard Test Method for Measurement of Magnetically Induced Torque on Medical Devices in the Magnetic Resonance Environment*. ASTM; 2021.
21. Zilberti L, Arduino A, Bottauscio O, Chiampi M. The underestimated role of gradient coils in MRI safety. *Magn Reson Med*. 2017;77:13-15.
22. Winter L, Seifert F, Zilberti L, Murbach M, Ittermann B. MRI-related heating of implants and devices: a review. *J Magn Reson Imaging*. 2021;53:1646-1665.
23. CST software website. Accessed April 9, 2024. https://www.3ds.com/products/simulia/cst-studio-suite.
24. Arduino A, Baruffaldi F, Bottauscio O, et al. Computational dosimetry in MRI in presence of hip, knee or shoulder implants: do we need accurate surgery models? *Phys Med Biol*. 2022;67:245022.
25. Ansys Mechanical software website. Accessed April 9, 2024. https://www.ansys.com/.
26. Zdero R, Brzozowsky P, Schemitsch EH. Biomechanical properties of artificial bones made by sawbones: a review. *Med Eng Phys*. 2023;118:104017.
27. Zilberti L, Bottauscio O, Chiampi M. A potential-based formulation for motion-induced electric fields in MRI. *IEEE Trans Magn*. 2016;52:1-4.
28. Zilberti L, Bottauscio O, Chiampi M. Assessment of exposure to MRI motion-induced fields based on the international commission on non-ionizing radiation protection (ICNIRP) guidelines. *Magn Reson Med*. 2016;76:1291-1300.
29. Gosselin MC, Neufeld E, Moser H, et al. Development of a new generation of high-resolution anatomical models for medical device evaluation: the virtual population 3.0. *Phys Med Biol*. 2014;59:5287-5303.
30. Viceconti M, Monti L, Muccini R, Bernakiewicz M, Toni A. Even a thin layer of soft tissue may compromise the primary stability of cementlesship stems. *Clin Biomech*. 2001;16:765-775.
31. Ghoul WE, Chidiac JJ. Prosthetic requirements for immediate implant loading: a review. *J Prosthodont*. 2012;21:141-154.
32. Van Arkel RJ, Ghouse S, Milner PE, Jeffers JRT. Additive manufactured push-fit implant fixation with screw-strength pull out. *J Orthop Res*. 2018;36:1508-1518.
33. Gao X, Fraulob M, Haiat G. Biomechanical behaviours of the bone–implant interface: a review. *J R Soc Interface*. 2019;16:20190259.
34. Kohli N, Stddart JC, Van Arkel RJ. The limit of tolerable micromotion for implant osseointegration: a systematic review. *Sci Rep*. 2021;11:10797.
35. Immel K, Nguyen VH, Haiat G, Sauer RA. Modeling the debonding process of osseointegrated implants due to coupled adhesion and friction. *Biomech Model Mechanobiol*. 2023;22:133-158.
36. Chong DYR, Hansen UN, Amis AA. Analysis of bone–prosthesis interface micromotion for cementless tibial prosthesis fixation and the influence of loading conditions. *J Biomech*. 2010;43:1074-1080.
37. Bergmann G, Deuretzbacher G, Heller M, et al. Hip contact forces and gait patterns from routine activities. *J Biomech*. 2001;7:859-871.
38. Kutzner I, Heilein B, Graichen F, et al. Loading of the knee joint during activities of daily living measured in vivo in five subjects. *J Biomech*. 2010;43:2164-2173.

How to cite this article: Zilberti L, Curreli C, Arduino A, Zanovello U, Baruffaldi F, Bottauscio O. Gradient-induced vibrations and motion-induced Lenz effects on conductive nonmagnetic orthopedic implants in MRI. *Magn Reson Med*. 2025;93:341-352. doi: 10.1002/mrm.30263